ORNL/TM-10904

OAK RIDGE NATIONAL LABORATORY

MARTIN MARIETTA

Sources of Compensation in Hadronic Calorimeters

M. S. Goodman
T. A. Gabriel
A. Di Ciaccio
R. Wilson

OAK RIDGE NATIONAL LABORATORY
CENTRAL RESEARCH LIBRARY
CIRCULATION SECTION
4500N ROOM 175
LIBRARY LOAN COPY
DO NOT TRANSFER TO ANOTHER PERSON
If you wish someone else to see this report, send in name with report and the library will arrange a loan.

OPERATED BY
MARTIN MARIETTA ENERGY SYSTEMS, INC.
FOR THE UNITED STATES
DEPARTMENT OF ENERGY

Printed in the United States of America. Available from
National Technical Information Service
U.S. Department of Commerce
5285 Port Royal Road, Springfield, Virginia 22161
NTIS price codes—Printed Copy: A03; Microfiche A01

This report was prepared as an account of work sponsored by an agency of the United States Government. Neither the United States Government nor any agency thereof, nor any of their employees, makes any warranty, express or implied, or assumes any legal liability or responsibility for the accuracy, completeness, or usefulness of any information, apparatus, product, or process disclosed, or represents that its use would not infringe privately owned rights. Reference herein to any specific commercial product, process, or service by trade name, trademark, manufacturer, or otherwise, does not necessarily constitute or imply its endorsement, recommendation, or favoring by the United States Government or any agency thereof. The views and opinions of authors expressed herein do not necessarily state or reflect those of the United States Government or any agency thereof.

ORNL/TM-10904

Engineering Physics and Mathematics

Sources of Compensation in Hadronic Calorimeters

M. S. Goodman*
T. A. Gabriel
A. Di Ciaccio+
R. Wilson†

DATE PUBLISHED —DECEMBER 1988

*Bell Commun. Research, Morristown, NJ
+CERN/INFN/University of "Tor Vergata" of Roma
†Dept. of Physics, Harvard University

NOTICE: This document contains information of a preliminary nature. It is subject to revision or correction and therefore does not represent a final report.

Prepared by the
OAK RIDGE NATIONAL LABORATORY
Oak Ridge, Tennessee 37831
operated by
MARTIN MARIETTA ENERGY SYSTEMS, INC.
for the
U.S. DEPARTMENT OF ENERGY
under contract DE-AC05-84OR21400

MARTIN MARIETTA ENERGY SYSTEMS LIBRARIES
3 4456 0283942 7

CONTENTS

ABSTRACT v
1. INTRODUCTION 1
2. METHOD OF CALCULATION 3
3. RESULTS 7
4. CONCLUSIONS 12
REFERENCES 14

ABSTRACT

Monte Carlo simulations are presented using the CALOR code system to study the design of a large hybrid hadron calorimeter system employing a warm liquid active medium (tetramethylsilane, $Si(CH_3)_4$) and uranium plates in addition to a conventional Fe/plastic system. In the system described here, the uranium provides partial compensation by suppressing the electromagnetic cascade produced by incident electrons due to sampling inefficiencies. The results of the simulations also indicate that significant compensation is achieved (given small enough saturation) due to low energy recoil protons produced in collisions with low energy (1-20 MeV) cascade and fission neutrons in the active medium. Both compensation mechanisms are important to help balance the response of a calorimeter to incident electrons and hadrons, that is, to achieve a ratio of pulse heights (e/h $\approx$1) which will lead to the best energy resolution.

1. INTRODUCTION

Hadron calorimeters based on sampling hadron showers in liquid active media are attractive since they provide uniformity of signal response and ease of calibration. Calorimeters based on the use of liquid argon have achieved reasonably good hadron energy resolution;[1,2] however, for large calorimeters the low temperatures required for liquid argon (~80K) necessitate complex and costly cryogenic arrangements. Thus, there has been growing interest in the use of warm liquids for large hadron calorimeters. Two potential candidate materials are Tetramethylsilane (TMS) and Tetramethylpentane (TMP). Results of Monte Carlo studies are presented of the response of a large hybrid hadron calorimeter based on TMS and uranium plates in the front, with an Fe/plastic rear calorimeter. The results of these calculations were used for the initial design of a calorimeter at CERN.[3] A preliminary report of these calculations has been published elsewhere.[4]

The first requirements of a hadron calorimeter design are to make it large enough to contain most of the hadronic shower and to have enough samples that sampling fluctuations are small. Assuming these, the two most important parameters of a hadron calorimeter, the energy resolution and the ratio of the most probable signal from an electron to that from a hadron of the same energy (e/h) will be dominated by fluctuations in the hadron shower and losses due to nuclear binding energy. In calorimeter design it is usually assumed that the active medium samples the shower in the passive medium in detail and that for both the incident radiation, and the secondary radiation, the signal output from the active medium is the same fixed fraction of the energy deposited in the passive medium. While this is approximately true for electromagnetic calorimeters, it is far from the truth for hadron calorimeters. In practice, however, the active and passive media exhibit different characteristics when exposed to similar types of radiation. The active media often do not give similar response for the same energy deposition by different particles and the energy sampling is not equal in the active region for electrons, low-energy neutrons, and gamma rays. Calorimeters which utilize iron or low atomic weight (A) materials as the passive media exhibit an almost equal distribution of the cascade energy into protons, neutrons, charged pions and neutral pions for intermediate incident energy (1-20 GeV) hadrons. On the contrary, if Pb, Ta, or U is used as the passive material, the energy distribution among produced particles is shifted toward additional neutron production through spallation and fission. There are more secondary particles and the energy spectra of all of them are shifted toward lower energies. In calorimeters utilizing low A materials, the majority of the signal is from charged particles which are produced in the passive material and which pass through the active region. In calorimeters utilizing high A material, the signal from charged particles produced in the passive material is reduced relative to the energy deposition due to the neutral particles, in particular, low energy cascade neutrons of energy 1-20 MeV. To fully utilize the sizable fraction of energy left in the cascade due to these neutrons of energy less than 20 MeV, the detection medium itself must be sensitive through internal collisions with these particles. It is also possible to deliberately enhance the signal due to these low energy neutrons, relative to the signal from other particles by using an active medium which detects these neutrons with greater efficiency than the passive medium.

One way of enhancing this sensitivity to low energy neutrons is by using a hydrogenous active medium.[4,5,6] Hydrogen has a large cross section for neutron scattering, on the order of several $\times\ 10^{-24}$ cm^2 for neutrons of energy of a few MeV. Hydrogen also allows for the largest energy transfer considering elastic scattering.[4,5,6] Proton production via nonelastic neutron collision with other nuclei in the active media will only consume binding energy and will not help substantially with the signal. With equal sensitivity of the active media to gamma rays, electrons, and neutrons, it can be shown that the choice of a hydrogenous active medium and a passive medium with high atomic number can overcompensate for the loss of hadron pulse height due to nuclear binding energy and lead to an e/h ratio less than unity. On the other hand, low energy recoil protons of a given energy produce in many detectors, a smaller signal than electrons or gamma rays of the same energy thereby reducing their effectiveness. (This is illustrated in Fig. 2.)

The use of uranium, as first suggested by Fabjan and Willis[1] offers a way to compensate and improve the resolution on an event-by-event basis for hadronic shower fluctuations and losses due to nuclear binding energy. The understanding of this compensation and improved resolution was initially not correctly understood.[3,4,5,6] These improvements can be understood from an examination of the hadronic cascade. If the particle cascade is strongly electromagnetic in character, that is, there is extensive production of neutral pions which decay into photons, the uranium will tend to suppress the electromagnetic part of the cascade due to sampling inefficiencies, that is, a larger fraction of the energy will be deposited in the U than would be expected by a simple analysis. However, if the cascade is strongly hadronic, there will be an amplification of the low energy neutron and to a lesser extent gamma ray energy available due to hadronically produced casade neutrons and fission neutrons, and neutron induced fission, capture, and inelastic collisions leading to the emission of fission and capture gamma rays. Sampling inefficiences are not as large for pure hadronic cascades, therefore the signal remains less affected. The combination of electromagnetic suppression and little hadronic suppression improves the resolution by narrowing the pulse height. However, if the active medium is not very sensitive to low energy neutrons only sampling inefficiencies will contribute to improvements in compensation; i.e., improvements in the e/h ratio. If liquid argon is chosen as the active medium, signals from the low energy neutron collisions with the argon atoms will be greatly suppressed due to saturation effects and small energy transfers.[4,5,6] If plastic, TMS, or TMP is chosen, the hydrogen will enable the low energy neutrons to produce proton recoils. However, saturation effects due to the inefficient light or charge production mechanism for low energy protons can limit their effectiveness. The liquid argon should be somewhat better for the detection of the low energy gamma rays due to its larger atomic number.[5,6] The use of a hydrogenous warm liquid, such as TMS or TMP would be an attempt to gain the best of both types of detectors: the uniformity of response characteristic of liquid argon, and the ability to detect low energy proton recoils of the plastic scintillator.

Presented in the following sections are a brief description of the code system and the method of calculation used, and a description of the results of the simulations of the hybrid calorimeter system.

2. METHOD OF CALCULATION

The calculations were performed with the CALOR computer system following approximately the procedures used in previous calculations.[6,7,8] A flow diagram of the codes in CALOR is given in Fig. 1. The three-dimensional, multimedia, high-energy nucleon-meson transport code, HETC,[9] was used, with modifications, to obtain a detailed description of the nucleon-meson cascade produced in the devices considered in this paper. This Monte Carlo code takes into account the slowing down of charged particles via the continuous slowing-down approximation, the decay of charged pions and muons, inelastic nucleon-nucleus and charged-pion-nucleus (excluding hydrogen) collisions through the use of the intermediate-energy intranuclear-cascade-evaporation (MECC) model (E < 3 GeV) and scaling model (E > 3 GeV), and inelastic nucleon-hydrogen and charged-pion-hydrogen collisions via the isobar model (E < 3 GeV) and phenomenlogical fits to experimental data (E > 3 GeV). Also accounted for are elastic neutron-nucleus (E < 100 MeV) collisions, and elastic nucleon and charged-pion collisions with hydrogen.

The intranuclear-cascade-evaporation models as implemented by Bertini is the heart of the HETC code.[10] This model has been used for a variety of calculations and has been shown to agree quite well with many experimental results. The underlying assumption of this model is that particle-nuclear interactions can be treated as a series of two-body collisions within the nucleus and that the location of the collision and resulting particles from the collision are governed by experimental and/or theoretical particle-particle total and differential cross-section data. The types of particle collisions included in the calculations are elastic, nonelastic and charge exchange. This model incorporates the diffuseness of the nuclear edge, the Fermi motion of the bound nucleons, the exclusion-principle, and a local potential for nucleons and pions. The density of the neutrons and protons within the nucleus (which is used with the total cross sections to determine interaction locations) are determined from the experimental data of Hofstadter.[10] Nuclear potentials are determined from these density profiles by using a zero-temperature Fermi distribution. The total well depth is then defined as the Fermi energy plus 7 MeV. Following the cascade part of the interaction, excitation energy remains in the nucleus. This energy is treated by using an evaporation model which allows for the emission of protons, neutrons, d, ^{3}He, α and T. Fission, induced by high-energy particles, is accounted for during this phase of the calculation by allowing it to compete with evaporation. Whether or not a detailed fission model is included has very little effect on the total number of secondary neutrons produced.

The source distribution for the electromagnetic cascade calculation is provided by HETC; it consists of photons from neutral pion decay, electrons and positrons from muon decay (although this is usually not of interest in calorimeter calculations because of the long muon lifetime), de-excitation gamma rays from nonelastic nuclear collisions and fission gamma rays. Since the discrete decay energies of the deexcitation gammas are not provided by HETC and only the total energy is known, individual gamma energies are obtained by uniformly sampling from the available energy until it is completely depleted. The transport of the electrons, positrons, and gammas from the above sources is carried out using the EGS system.[11]

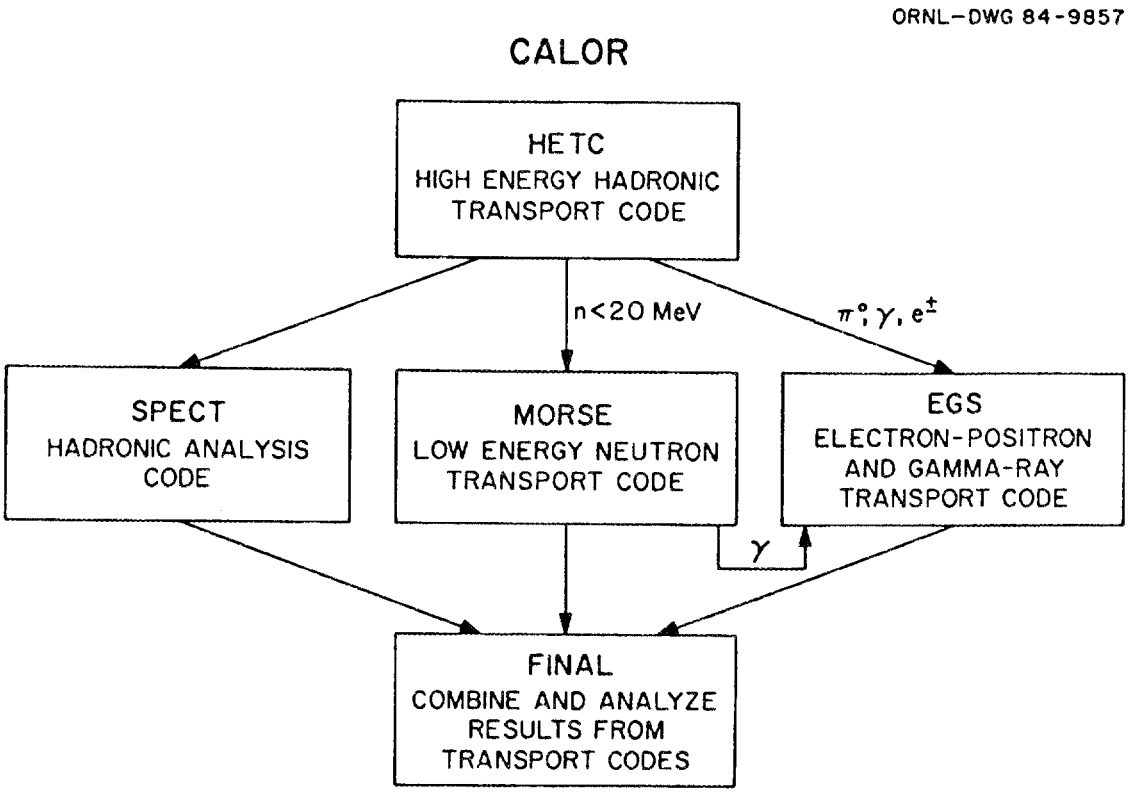

Figure 1. Flow diagram of the CALOR system.

Neutrons which are produced with energies below 20 MeV are transported using the MORSE[12,13] Monte Carlo transport code. The neutron cross sections used by MORSE were obtained from ENDFB/IV. Gamma rays (including those from capture, fission, etc.) produced during this phase of the calculations are stored for transport by the EGS code. The MORSE code was developed for reactor application and can treat fissioning sytems in detail. This ability is very important since a majority of the fissions results from neutrons with energies less than 20 MeV. Time dependence is included in MORSE, but since neither HETC nor EGS has a timing scheme incorporated, it has been assumed that no time passes for this phase of the particle cascade. Therefore, all neutrons below 20 MeV are produced at t = 0. General time cuts used in the MORSE code are 50 ns for scintillator and 100 ns for TMS although studies were also performed with times as long as 400 nsec.

The nonlinearity of the light pulse, L, in scintillator due to saturation effects is taken into account by the use of Birk's law,[14]

$$\frac{dL}{dx} \propto \frac{dE/dx}{1 + k_B dE/dx},$$

where k_B is the saturation constant. For the plastic scintillator, k_B has been taken to be 0.01 g cm^2 MeV^{-1}. A similar law is assumed to apply to the charge collected in ionization detectors. This takes into account the loss of signal resulting from recombination effects in the ionization column.[15] A variety of k_B values have been considered in this study of TMS since, at present, this media has not been well investigated. For electrons at all energies, it is assumed that $k_B = 0$. An example of these data are given in Fig. 2.

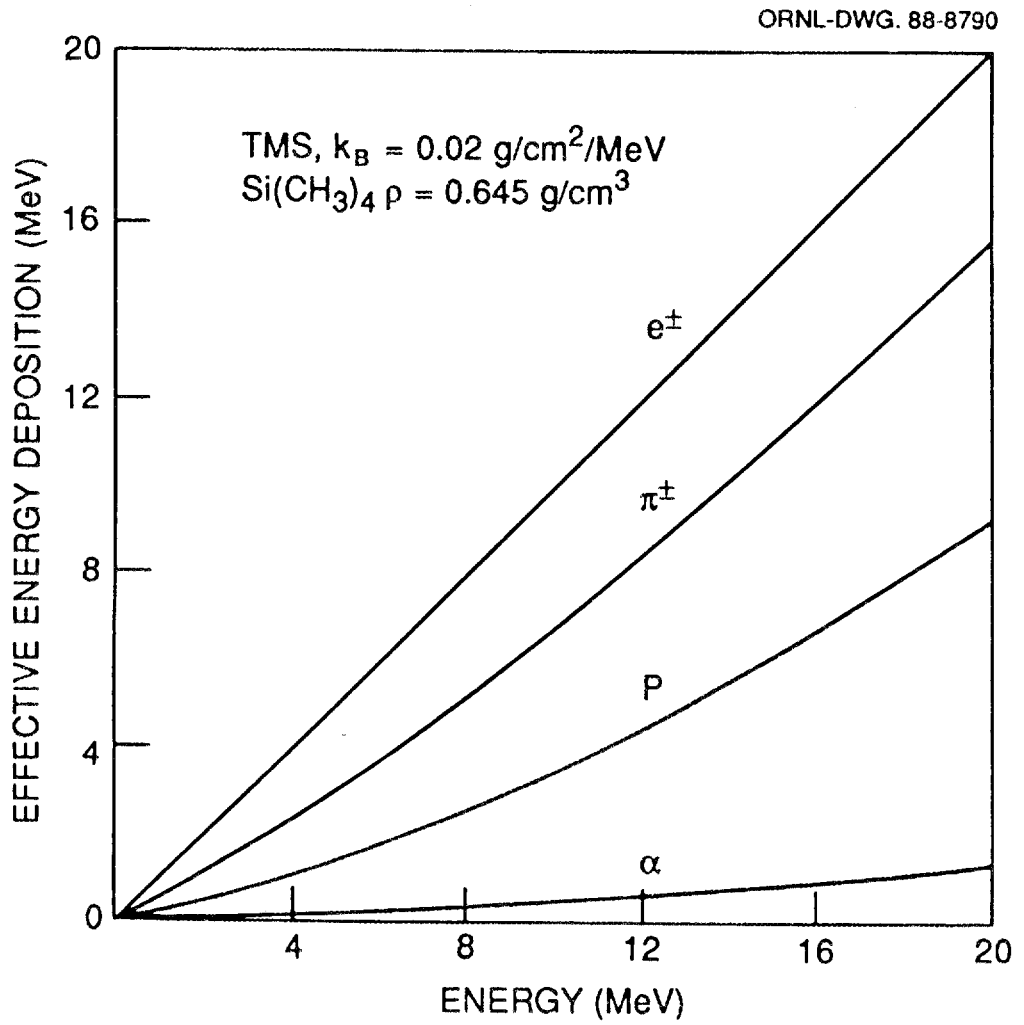

Figure 2. Effective energy deposition vs. charged particle energy for several different types of particles. Similar curves are used for plastic scintillator.

3. RESULTS

The results of calculations are discussed for Fe/TMS, Pb/TMS and U/TMS front calorimeters, combined with Fe/plastic rear calorimeters. (These calculations were prepared for an upgrade of the UA-1 calorimeter system, and as such had size constraints imposed due to that specific experiment geometry.[3]) The results provide insights into compensation effects due to the large hydrogen content of the TMS, and due to electromagnetic sampling inefficiencies even though the calorimeter as simulated does have sizeable leakage from the front section. The geometry used in the calculations (see Fig. 3) are for plates of Fe, Pb, or U which are 2.0 mm thick, followed by TMS of 2.0 mm thickness for a total depth of 0.448 m. Behind the TMS calorimeter is an iron/plastic calorimeter utilizing unit cells of 50 mm Fe and 10 mm plastic, repeated 14 times. The lateral extent completely contains the showers.

Table 1 indicates the calculated energy resolution for several geometrical configurations and energy categories. Although the hadronic cascade is not totally contained in the uranium section, there is nearly total containment when the signal from the Fe/Plastic sections are added to those from the U/TMS section. The resolution for 1 GeV hadrons is better than for 5 GeV hadrons due primarily to the fact that for 1 GeV showers, almost all the energy is contained in the front section of the calorimeter. One can infer from this single data point that the energy resolution of a long U/TMS device will be about $40\%/\sqrt{E}$ which is comparable to the resolution measured in plastic scintillator/uranium calorimeters.

Table 2 shows the fractional contribution of the different secondary particles to the total detected energy from a 5 GeV proton shower. The first row shows the fractional detected energy from the charged particles in the cascade and from the high energy neutrons. For this row, there is comparatively little saturation in either scintillator or ionization calorimeter for reasonable values of k_B.

The second row is the fractional detected energy due to neutrons of energy less than 20 MeV. These include both the spallation neutrons and the fission neutrons. However, since the fission neutrons have typical energies of 1-2 MeV, where the saturation effects are considerable, fission neutrons contribute only a small amount for this value of k_B ($= 5.45 \times 10^{-4}$ gm/cm^2/MeV). The large (61%) fraction for U/TMS is reduced considerably when a larger value of k_B is used.

The third row indicates the contribution due to gamma rays from slow fission and nuclear excitation. The fourth row indicates the energy in the high energy electromagnetic channel; this includes both gamma rays from fast fission and those resulting from neutral pion decay.

The fractional energy due to recoil protons (row 2) increases as A increases from Fe to Pb, and this large increase in the detected energy in combination with a decrease in the electron signal at the same incident energy causes a transition from undercompensation to overcompensation, at least at the indicated level of saturation. Since the number of spallation neutrons is proportional to A, this contribution begins to dominate the total energy deposition in TMS for large A. Although providing a few percent of the total energy deposited in the TMS, the contribution due to low-energy gamma rays, once thought to be the major compensation effect, is not dominant. The neutron-induced proton (and heavy ion) recoils dominate the total energy deposition for large A, and the large fluctuations

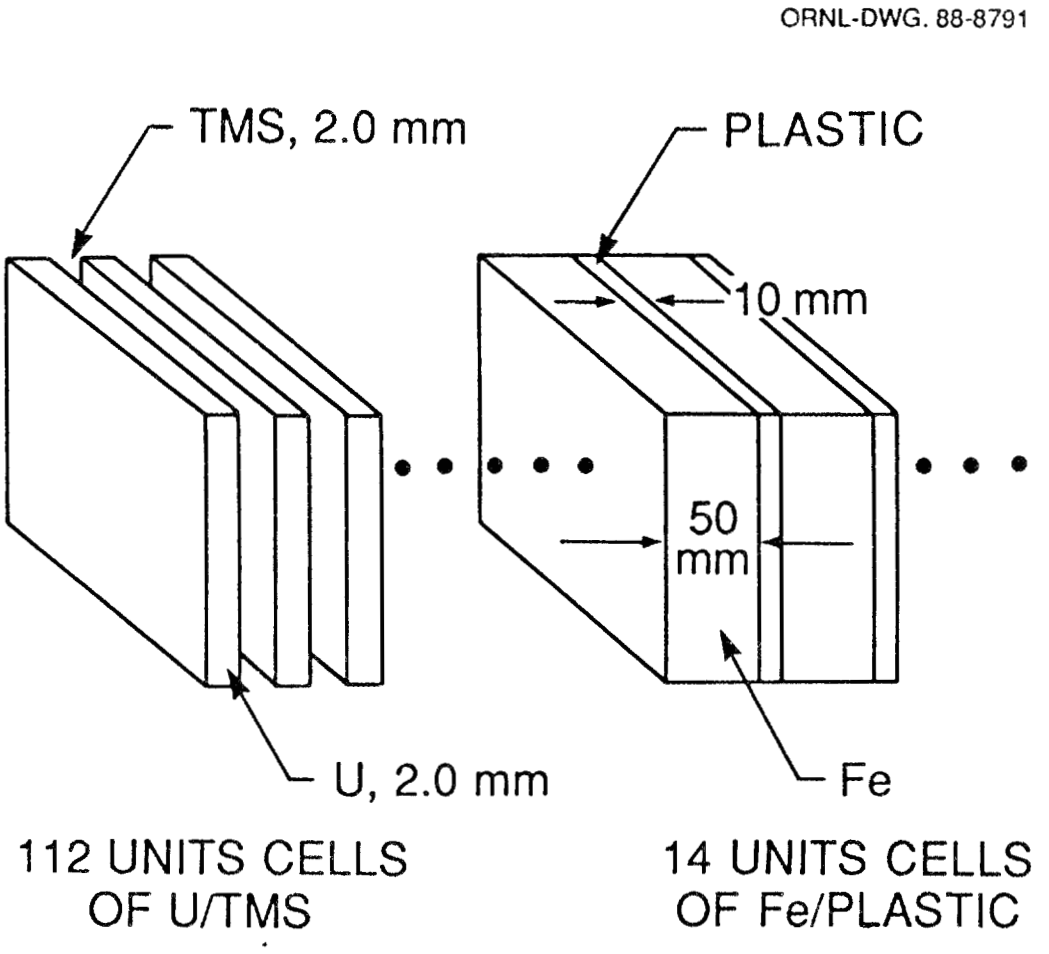

Figure 3. Geometry of the calorimeter. For some calculations the uranium plates were replaced by Fe, Pb, and U/Fe.

Table 1. Energy Resolutions in TMS Calorimeters for Incident Protons

Calorimeter*	Energy (GeV)	k_B gm/cm^2/MeV	$\sigma/\sqrt{E}(\%)$
U/TMS	5	5.45×10^{-4}	0.52
	1	5.45×10^{-4}	0.37
U/Fe/TMS	5	0.	0.45
	5	5.45×10^{-4}	0.45
	5	2.10×10^{-3}	0.40
Pb/TMS	5	5.45×10^{-4}	0.51

*Plus iron-plastic at rear. $k_B = 0.01$ gm/cm^2/MeV for the plastic.

Table 2. Fractional Detected Energy and e/h Ratios in the TMS Calorimeters for 5 GeV Protons*

	Fe/TMS	U/TMS	Pb/TMS
Primary p and secondary π, p, μ, nuclear-recoil, and evaporated-charged particles	0.57	0.27(0.32)†	0.41
Neutrons with energy <20 MeV	0.22	0.61(0.56)	0.43
De-excitation and fission gamma rays	0.024	0.039(0.033)	0.024
Electromagnetic from π° decay and fast fission and nonelastic gamma rays	0.18	0.072(0.086)	0.13
e/h	1.3	0.51(0.61)	0.92

*$k_B = 5.45 \times 10^{-4}$ gm/cm^2/MeV.

†No low energy fission allowed.

in this energy deposition dominate the energy resolution. The e/h ratio which includes the contribution due to the Fe/plastic calorimeter is also given. The energy deposition in the rear Fe/plastic scintillator calorimeter was added to the energy deposition in the uranium/TMS front calorimeter by a procedure which determined the sum of the energy in front and back sections in such a way that the overall energy resolution for all histories in a given run was minimized. The e/h ratios were determined by fitting the pulse height distributions with a Gaussian and using the average values. The quoted values are the ratio of the average values. The errors on e/h were determined by calculating the errors on the fitted parameters. The errors on e/h are <0.1 for all the cases studied.

The effect of various values of k_B on the e/h ratio are shown in Fig. 4. In the case of the Fe/TMS, complete compensationtion is not possible, regardless of the saturation value assumed. In U/TMS or U/Fe/TMS, it is possible depending on saturation level to overcompensate or undercompensate. The value of k_B has not yet been extensively measured. The best indication so far is $k_B = 0.02$ gm/cm^2/MeV. This comes from measurements of the pulse height from α particle ionization (where the ionization is heavily saturated) to that from cosmic rays (where it is not).[16] The value of k_B is expected to decrease with increasing electric field. If further research confirms this value of the saturation, complete compensation may not be possible with a TMS based device. In this case the energy deposition associated with the low energy neutrons will not be as effective as it would be given a smaller value of the saturation.

Since this work was performed, other calculations have been performed by Wigmans[17] and Albrow.[3] For best compensation using hydrogenous active media, it is desirable to make a sharp distinction between the hydrogenous active medium and the nonhydrogenous passive medium. This is best achieved when the thickness of the active medium is about the range of the recoil protons from the typical spallation neutrons. The calculations by Wigmans show compensation. The values chosen here (see Fig. 3) are (not entirely accidental) close to the values that Wigmans finds give the optimum compensation.

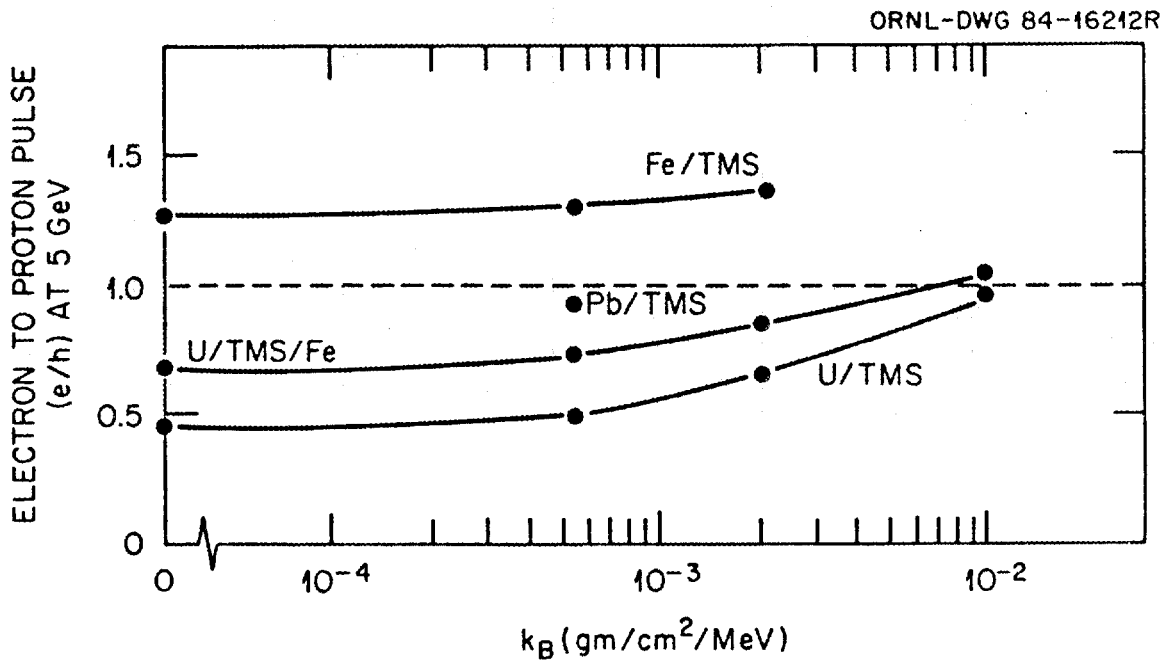

Figure 4. Electron-to-proton pulse ratio, e/h, at 5 GeV as a function of saturation level as given by Birk's constant k_B.

4. CONCLUSIONS

Several conclusions about calorimeter designs using warm conducting liquids may be drawn from this work. First, hydrogenous materials as active media will give substantially different response to hadron cascades than nonhydrogenous media because of the effect of recoil protons produced by low energy neutrons. In order to see this effect, the effective saturation of the hydrogenous media must be small. Although these studies were performed for TMS, the conclusions should apply to other hydrogenous media as well. The slow fission contribution, that is, the contribution to the total energy deposition due to uranium fissions caused by neutrons below 20 MeV, although a few percent of the total energy deposited, is not the dominant source of compensation. The factor which is dominant is the production of spallation neutrons, an effect which increases with increasing A. Therefore, some compensation appears possible without the use of fissionable material. Whether this compensation is achievable, in practice, will depend strongly on the attainable saturation values of the active media and the level of electromagnetic sampling inefficiency.

Acknowledgements

The authors would like to thank C. Rubbia for pointing out the need for these calculations, R. Munoz for giving us the results of his nonlinearity measurements prior to publications, and C. Fabjan and R. Willis for helpful comments and discussions.

REFERENCES

1. C. W. Fabjan et al., *Nucl. Instrum. & Methods* **141**, 61 (1977).
2. O. Botner et al., *IEEE Trans. Nucl. Sci.*, NS-28 (1981) 510.
3. M. G. Albrow et al., *Nucl. Instrum. & Methods* **A265**, 303 (1988).
4. T. A. Gabriel et al., *IEEE Trans. Nucl. Sci.* **NS-32**, 1 (1985).
5. J. E. Brau and T. A. Gabriel, SLD - New Detector Note No. 119 (May 22, 1984).
6. J. Brau and T. A. Gabriel, *Nucl. Instrum. & Methods* **238**, 489 (1985).
7. T. A. Gabriel and W. Schmidt, *Nucl. Instrum. & Methods* **134**, 271 (1976).
8. T. A. Gabriel, *Nucl. Instrum. & Methods* **150**, 146 (1978).
9. T. A. Gabriel, "The High Energy Transport Code HETC," Oak Ridge National Laboratory, ORNL/TM-9727 (1985).
10. H. W. Bertini, *Phys. Rev.* **188**, 1711 (1969).
11. R. L. Ford and W. R. Nelson, Stanford Linear Accelerator Center, SLAC-0210 (1978).
12. M. B. Emmett, ORNL-4972, Oak Ridge National Laboratory (1975).
13. N. M. Greene et al., ORNL/TM-3706, Oak Ridge National Laboratory (1973).
14. J. B. Birks, *Proc. Phys. Soc.* **A64**, 874 (1951).
15. A. Babaev et al., *Nucl. Instrum. & Methods* **160**, 427 (1979).
16. Munoz, private communication.
17. R. Wigmans, *Nucl. Instrum. & Methods* **A259**, 376 (1987).

INTERNAL DISTRIBUTION

1. F. S. Alsmiller
2. R. G. Alsmiller, Jr.
3. B. R. Appleton
4. D. E. Bartine
5. B. L. Bishop
6–10. T. A. Gabriel
11. J. K. Ingersoll
12. R. A. Lillie
13. F. C. Maienschein
14. RSIC
15–19. C. Zeigler
20. EPMD Reports Office
21–22. Laboratory Records Department
23. Laboratory Records, ORNL-RC
24. Document Reference Section
25. Central Research Library
26. ORNL Patent Section

EXTERNAL DISTRIBUTION

27. Office of the Assistant Manager for Energy Research and Development, Department of Energy, Oak Ridge Operations, P.O. Box 2001, Oak Ridge, TN 37831
28. Argonne National Laboratory, Library Services Dept., 302-CE125, 9700 S. Cass Avenue, Argonne, IL 60439
29. T. W. Armstrong, Science Applications, Inc., PO Box 2807, La Jolla, CA 92038
30. Miguel Awschalom, National Accelerator Laboratory, PO Box 500, Batavia, IL 60510
31. V. S. Barashenkov, Laboratory of Theoretical Physics, Joint Institute for Nuclear Research, Head Post Office, PO Box 79, Moscow, USSR
32. Gerald W. Bennett, Brookhaven National Laboratory, Upton, NY 19973
33. D. Berley, National Science Foundation, Washington, DC 20550
34. Elliott Bloom, Stanford Linear Accelerator Center, PO Box 4349, Stanford, CA 94305
35. J. Brau, University of Oregon, Eugene, OR 97403
36. Bruce Brown, Fermi National Accelerator Laboratory, PO Box 500, Batavia, IL 60510
37. David O. Caldwell, Dept. of Physics, University of California at Santa Barbara, Santa Barbara, CA 93106
38. Stanley B. Curtis, Lawrence Radiation Laboratory, Bldg. 29, Room 213, Berkeley, CA 94720
39. Herbert DeStaebler, Stanford Linear Accelerator Center, Stanford University, Stanford, CA 94305
40. A. Di Ciaccio, CERN, Geneva 23, Switzerland
41. J. J. Dorning, Dept. of Nucl. Eng. and Engineering Physics, University of Virginia, Charlottesville, VA 22901
42. R. D. Edge, Physics Dept., University of South Carolina, Columbia, SC, 29208
43. R. Eisenstein, Dept. of Physics, University of Illinois, Urbana, IL 61801
44. R. W. Ellsworth, George Mason University, Fairfax, VA 22030
45. Chris Fabjan, CERN, Geneva 23, Switzerland
46. G. Feldman, Stanford Linear Accelerator Center, Stanford University, Stanford, CA 94305

47. W. T. Ford, Experiment 1A-Lab C, Fermi National Accelerator Laboratory, PO Box 500, Batavia, IL 60510
48. E. Fowler, Dept. of Physics, Purdue University, West Lafayette, IN 47907
49. H. T. Freudenreich, University of Maryland, College Park, MD 20742
50. E. Freytag, Deutsches Elektronen-Synchrotron, DESY, 2 Hamburg Dr., Flottbek, Notkesteig 1, W. Germany
51. M. G. D. Gilchriese, SSC Central Design Group, Lawrence Berkeley Laboratory, Berkeley, CA 94720
52. G. T. Gillies, Dept. of Physics, University of Virginia, Charlottesville, VA 22901
53. G. E. Gladding, University of Illinois, Dept. of Physics, Urbana, IL 61801
54. K. Goebel, Health Physics Group, CERN, 1211 Geneva 23, Switzerland
55. J. A. Goodman, University of Maryland, College Park, MD 20742
56. M. Goodman, Bell Communication Research, Morristown, NJ 07960
57. D. Groom, SSC Central Design Group, Lawrence Berkeley Laboratory, Berkeley, CA 94720
58. Herman Grunder, Deputy Director, General Sciences, Lawrence Berkeley Laboratory, Bldg. 50A, Room 4119, 1 Cyclotron Rd., Berkeley, CA 94720
59. H. J. Hargis, University of Tennessee, Dept. of Physics, Knoxville, TN 37919
60. Frenc Hajnal, Health and Safety Laboratory, U.S. Department of Energy, 376 Hudson St., New York, NY 120014
61. R. M. Haralick, Dept. of Electrical Engineering, University of Washington, Seattle, WA 98195
62. M. Hofert, CERN, 1211 Geneva 23, Switzerland
63. Terrence Jensen, Dept. of Physics and Astronomy, The University of Rochester, Rochester, NY 14627
64. D. Lal, Tata Institute of Fundamental Research, National Centre of the Government of India, for Nuclear Science & Mathematics, Homi Bhabha Rd.,, Bombay 5, India
65. Lawrence Livermore Laboratory, Technical Information Department, PO Box 808, Livermore, CA 94550
66. V. Lebedev, Institute of High Energy Physics, Serpukhov, Moscow Region, USSR
67. Library for Nuclear Science, Massachusetts Institute of Technology at Middleton, Middleton, MA 01949
68. J. LoSecco, Dept of Physics, California Institute of Technology, Pasadena, CA 91125
69. J. Marks, Accelerator Fusion Research Division, Lawrence Berkeley Laboratory, Bldg. 50, Room 149, 1 Cyclotron Rd., Berkeley, CA 94720
70. A. I. Mincer, University of Maryland, College Park, Md 20742
71. V. S. Narashimham, Tata Institue of Fundamental Research, Bombay 400 005,, India
72. W. R. Nelson, Stanford Linear Acclerator Center, Stanford University, PO Box 4349, Stanford, CA 94305
73. T. R. Palfrey, Jr., Dept. of Physics, Purdue University, West Lafayette, IN 47907
74. Robert Palmer, Brookhaven National Laboratory, Upton, NY 11973
75. C. W. Peck, Dept. of Physics, California Institute of Technology, Pasadena, CA 91109

76. J. Ranft, Karl-Marx University, Physics Section, Linnestrasse 5, 701, Leipzig, E. Germany
77. Lincoln Read, Division of High Energy & Nuclear Physics, Department of Energy, Washington, DC 20545
78. Jim Reidy, University of Mississippi, University, MS 38677
79. C. Rubbia, Lyman Laboratory, Harvard University, Cambridge, MA 02138
80. W. Schmidt, Institute of Experimental Nuclear Physics, University of Karlsruhe, 75 Karlsruhe, W. Germany
81. The Secretary, Radiation Group, Lab II, CERN, 1211 Geneva 23, Switzerland
82. Walter Selove, University of Pennsylvania, Dept. of Physics, Philadelphia, PA 19104
83. B.S.P. Shen, Dept. of Astronomy, University of Pennsylvania, Philadelphia, PA 19104
84. M. Shupe, Dept. of Physics, University of Minnesota, Minneapolis, MN 55455
85. Alan Stevens, Physics Dept., Brookhaven National Laboratory, Upton, NY 11973
86. G. R. Stevenson, Radiation Protection Group, Lab II, CERN, 1211 Geneva 23, Switzerland
87. L. Sulak, Dept. of Physics, University of Michigan, Ann Arbor, MI 48109
88. R. F. Taschek, Los Alamos National Laboratory, PO Box 1663, Los Alamos, NM 87544
89. R. Tesch, DESY, Hamburg, Notkesteig 1, W. Germany
90. R. H. Thomas, Lawrence Radiation Laboratory, Health Physics Dept., Bldg. 72, Berkeley, CA 94720
91. V. D. Toneev, Laboratory of Theoretical Physics, Joint Institute for Nuclear Research, Head Post Office, PO Box 79, Moscow, USSR
92. S. C. Tonwar, University of Maryland, College Park, Md 20742
93. W. Tuchinetz, Massachusetts Institute of Technology, R26-411, Cambridge, MA 02139
94. Jim Walker, University of Florida, Gainesville, FL 32611
95. W. J. Willis, CERN, Geneva 23, Switzerland
96. D. Winn, Lyman Laboratory, Harvard University, Cambridge, MA 02138
97. J. Wilczynski, Nuclear Research Center, Karlsruhe, W. Germany
98. S. Yellin, Stanford University, Stanford Linear Accelerator Center, PO Box 4349, Stanford, CA 94305
99. G. B. Yodh, University of Maryland, College Park, MD 20742
100. S. Youssef, SCRI, Florida State University, Tallahassee, FL 32306
101. B. Zeitnitz, Nuclear Research Center, Karlsruhe, W. Germany

102–111. Office of Scientific and Technical Information, PO Box 62, Oak Ridge, TN 37830